Indian Journal of Pure & Applied Physics
Vol. 52, April 2014, pp. 262-270

Electronic microscopic, thermal and electrical properties of $Bi_2V_{1-x}Ti_xO_{5.5-\delta}$ ($0.05 \leq x \leq 0.20$) oxide ion conductors

Gurbinder Kaur[a]*, O P Pandey[b] & K Singh[b]

[a]Department of Material Science and Engineering, Holden Hall, Virginia Tech, Blacksburg, Virginia-24060, USA

[b]School of Physics & Materials Science, Thapar University, Patiala 147 004, Punjab (India)

*E-mail: gkaur82@vt.edu

Received 3 July 2013; revised 30 September 2013; accepted 12 February 2014

In the present study, the effect of titanium substitution for vanadium on oxide ion conductivity, phase stability and thermal expansion has been investigated. The exact solid solubility limit of the dopant and its effect on conductivity as well as thermal expansion, have been studied. The samples have been prepared by conventional solid-state technique. The sintered samples were characterized using differential thermal analysis (DTA), thermo-gravimetric analysis (TGA), X-ray diffraction (XRD) and scanning electron microscopy (SEM). Sample $x = 0.20$ has shown maximum conductivity of 1.2×10^{-3} S/cm with minimum activation energy of 0.19 eV at 800°C. Along with this, maximum thermal expansion coefficient (TEC) is observed for $x = 0.2$ sample. The microstructures of the samples exhibited variation in grain size and porosity.

Keywords: Bismuth vanadate, Thermal expansion coefficient, Differential thermal analysis, Conductivity, Microstructure

1 Introduction

Bismuth vanadate $Bi_2VO_{5.5-\delta}$ is a favourable oxide ion electrolyte conductor for intermediate temperature solid oxide fuel[1-3] cell (IT-SOFC). $Bi_2VO_{5.5-\delta}$ consists of alternate bismuth-oxygen (Bi-O) and vanadium oxygen (V-O) layers. Bi-O layer in $[Bi_2O_2]^{2+}$ exhibits square pyramidal co-ordination for bismuth. Stereochemical activity of non-bonding $6s^2$ lone pairs of Bi contributes for its asymmetric coordination geometry. Electroneutrality of the system is preserved by VO_6 octahedrons[4,5] present in V-O layer $[VO_{3.5\ 0.5}]$. $Bi_2VO_{5.5-\delta}$ exhibits three different structures in temperature range from room temperature to 900°C whose crystalline structures are explained using sub-cell[2,5-7] of $a_m = 0.55$, $b_m = 0.56$ and $c_m = 1.53$ nm. At low temperature (< 445°C) monoclinic α phase is reported, which is generally *n*-type semiconductor having unit cell volume of $3a_m\times b_m\times c_m$. At intermediate temperature (445°-570°C) orthorhombic β phase, which is oxide ion conductor having unit cell volume of $2a_m\times b_m\times c_m$ is formed whereas at high-temperature (≈ 700°C) tetragonal γ phase is observed, which is an oxide ion conductor having volume of $(a_m/\sqrt{2})\times(a_m/\sqrt{2})\times c_m$.

Among these three primary phases, γ phase exhibits the highest conductivity whereas V-O layer is made up of corner-sharing oxygen octahedrons that contain oxygen vacancies. The kinetic stabilization of γ phase at room temperature has been the key issue for researchers[6-13]. Different dopants are being used to stabilize the main conducting γ phase at room temperature so as to increase conduction[6,7]. The compounds BIMEVOX (where BI represents bismuth, ME represents the dopant ion, V is the vanadium atom and OX represents oxygen) is the combined depiction of a large family of compounds where ME can be Cu, Ni, Ti, Pb, Zn, Fe, Al, Sb and Nb etc. are used to increase the ionic conductivity by stabilizing γ phase at room temperatures[8-13]. It is known that doping at vanadium site changes the phase transformation behaviour as well as electrical conductivity[7-15] of BIMEVOX.Aliovalent doping is expected to change the amount of oxygen vacancy to preserve electroneutrality. Moreover, the variation of size between vanadium and dopant induces lattice strain in BIMEVOX structure. The affinity between dopant and oxide ion can be described by lattice energy Q which is given by negative value of enthalpy change of following reaction:

$$A^{x+} + (x/2)O^{2-} \rightarrow AO_{x/2} \quad \ldots(1)$$

Dopant, which exhibits high Q value, binds more strongly with the oxide ion in BIMEVOX. These affinities between the atoms, which are influenced by the synthesis conditions, play a crucial role in determining the conductive properties and phase stabilization[1,16]. The phase transition behaviour, thermal analysis, expansivity and conductive

behaviour have been studied for $Bi_2V_{1-x}Ti_xO_{5.5-\delta}$ ($0.05 \leq x \leq 0.20$). Ti^{3+} exhibits six-fold octahedron having ionic radii of 0.67Å along with very high lattice energy[17] of 14.15 MJ/mol. In contrast to this, Ti^{4+} has ionic radii of 0.605Å and lattice energy 12.01 MJ/mol. Vanadium V^{5+} exhibits ionic radii of 0.054Å and lattice energy of 19.24 MJ/mol. Therefore, Ti_2O_3 has been chosen as an initial ingredient instead of TiO_2 due to its high lattice energy. Many researchers have reported that processing conditions can alter the properties significantly[8-10,18,19]. So, in the present study, the synthesis conditions have been changed to achieve higher density. In addition to this, the main objective of the present study is to know exact solid solubility limit of the dopant and its effect on conductivity and thermal expansion. Thermal expansion coefficient is very important parameter from the SOFC point of view that is not reported yet as far as our knowledge on these systems. Hence, detailed study of expansivity of these samples with respect to temperature has been done. The sintered samples were characterized using techniques like differential thermal analysis (DTA), thermo-gravimetric analysis (TGA), dilatometery, X-ray diffraction (XRD), *ac* conductivity and scanning electron microscopy (SEM).

2 Experimental Details

$Bi_2V_{1-x}Ti_xO_{5.5-\delta}$ ($0.05 \leq x \leq 0.25$) powders were prepared by solid-state reaction from stoichiometric amounts of the following oxides: Bi_2O_3 (99%), V_2O_5 (99%) and Ti_2O_3 (99.995%). In order to avoid contamination due to ball milling, the mixing was done using agate mortar and pestle for 2 h. The resulting mixtures were dried, ground and then calcined at 750°C in recrystallized alumina crucible for 12 h in air. Calcined powders were again ground and pelletized by compacting these powders in a hydraulic press at a load of 12 kN/cm^2. The pellets of 20 mm diameter and 5 mm thickness so prepared were sintered at 800°C for 12 h. The density of pellets was calculated using Archimedes principle. The XRD pattern of prepared samples was recorded using a PANalytical Xperts Pro. MPD diffractometer with CuK_α radiations. The pattern was recorded at a scanning rate of 2° min^{-1} with angular range of 20-70°. The DTA/TGA measurements were performed with Diamond Pyris TG/DTA (Perkin Elmer) using Al_2O_3 powder as reference material in oxygen atmosphere. The temperature and weight loss detection limit of the instrument are ± 1°C and 0.001 mg, respectively. The dilatometer study was done using Netzsch DIL 402 PC in the temperature range 50-800ºC to determine the TEC of prepared oxides. Electrical measurements in terms of complex impedance $Z(\omega) = Z'(\omega) - jZ''(\omega)$, were conducted on the gold sputtered pellets using *ac* impedance spectroscopy (Hewlett-Packard 4274A) equipped from 0.1 to 100 kHz and from room temperature to 800°C. Heating rate of 2°C/min was maintained to ensure a good attainment of equilibrium during measurement. The morphology and microanalysis of the samples have been done using SEM (EVO-ZEISS) and EDS.

3 Results and Discussion

3.1 X-ray diffraction (XRD)

The XRD pattern of $Bi_2V_{1-x}Ti_xO_{5.5-\delta}$ ($0.05 \leq x \leq 0.25$) is shown in Fig. 1(a). XRD data confirmed the presence of single phase in all samples except for $x = 0.25$. $Bi_2V_{0.75}Ti_{0.25}O_{5.5-\delta}$ oxide exhibited double phase i.e. BiVO4 phase precipitated out in addition to $Bi_2V_{0.75}Ti_{0.25}O_{5.5-\delta}$. $BiVO_4$ is a mixed conductor of electrons and oxide ions[20].

During long-term operation in SOFC, electronic conduction can lead to short-circuit. As the interest of present study is more focused on obtaining single phase, hence further investigation of $Bi_2V_{0.75}Ti_{0.25}O_{5.5-\delta}$ oxide was not done. In order to detect more precise solid solubility limit, $Bi_2V_{0.775}Ti_{0.225}O_{5.5-\delta}$ sample was also synthesized and characterized using XRD. This sample also exhibited mixed phase as indicated by X-ray diffractogram shown in Fig. 1(b). This further confirms the solid solubility limit up to $x = 0.2$. For $x = 0.05$ sample, the diffraction pattern is characterized by the presence of weak reflection at $2\Theta = 24.22°$. In addition to this, doublets have also been observed at $2\Theta = 31°$, 39°, 48° and 54°, which clearly indicate the presence of α, phase in this sample[2,21]. The XRD pattern of $x = 0.1$ shows the presence of two superlattice peaks at $2\Theta = 31.8°$ and 32.4° (with splitting). This further confirms the existence of β phase[22,23] for $x = 0.1$. On the other hand, $x = 0.15$ and 0.2, the XRD pattern does not show any super lattice diffraction peaks confirming the presence of γ phase in these samples[24]. Along with this, the shift in peaks has also been observed towards higher diffraction angles with the increase in dopant concentration, which could be attributed to the strain induced in lattice. For $x = 0.25$, the shift of peaks has occurred towards lower diffraction angle. Using Debye Scherrer's formula,

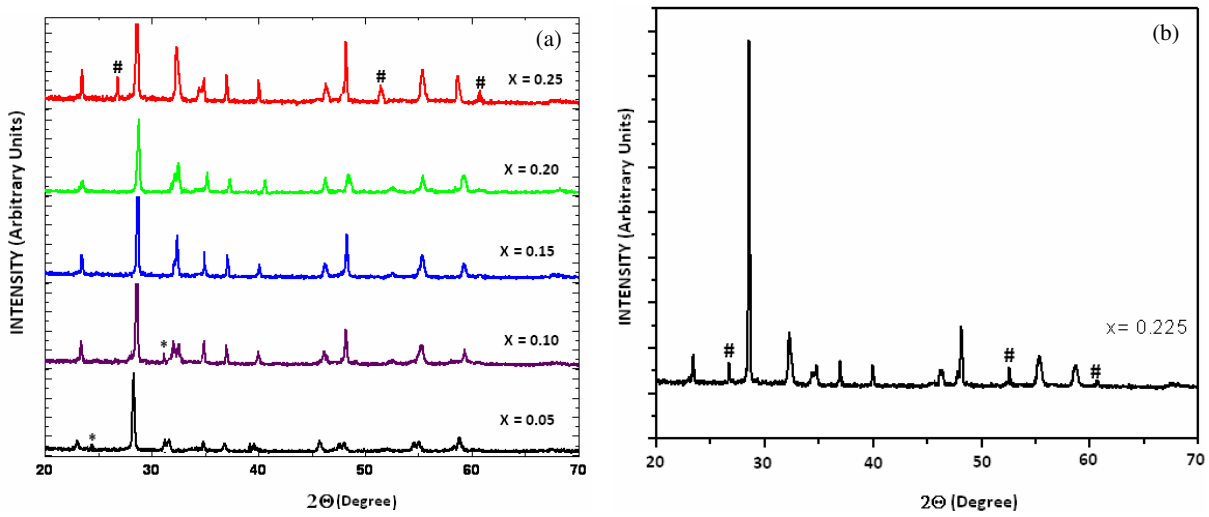

Fig. 1 — XRD spectrum obtained for the samples (a) $Bi_2V_{1-x}Ti_xO_{5.5-\delta}$ ($0.05 < x < 0.25$) and (b) for $x = 0.225$ [*-superlattice reflection, #-$BiVO_4$ phase]

the crystallite sizes have been calculated for all the doped samples. According to Debye-Scherrer's formula, the crystallite size is given by:

$$B = k\lambda/s\cos\theta \quad \ldots(2)$$

where B is the line width at half maximum, k is constant with value 0.94, λ is the wavelength of X-ray taken (λ = 1.54 Å), θ is the diffraction angle and s is the crystallite size. The crystallite size is obtained to be 23.8, 24.3, 23.1, 23.6 and 20.2 nm, respectively for sample x = 0.05, 0.1, 0.15, 0.20 and 0.25, respectively. For x = 0.25, smallest crystallite size is observed whereas for other compositions the crystallite size is more or less the same.

For further confirmation of γ-phase stabilization, heating and cooling cycles of DTA was performed.

3.2 Differential thermal analysis (DTA)

DTA was performed in order to determine the physical and chemical transformations during thermal cycling and check their stability in such conditions. Figure 2(a-d) shows the DTA profiles and differential DTA of all samples along with their weight change (shown in inset) during heating and cooling cycle. Differential method is advantageous as it allows peak detection even in the case of raw data. Furthermore, when the peak is overlapped with another peak at its shoulder, then it makes peak detection difficult which can be resolved with the help of differential DTA. In addition to this, the data obtained has baseline correction, which makes the detection of peaks easy.

For x = 0.05 sample [Fig. 2(a)], two endothermic peaks at 418°C and 529°C have been observed during heating cycle. The peak at 418°C corresponds to transition from α to β phase (α/β) whereas endotherm at 529°C represents phase transition[25] from β to γ phase (β/γ). The exothermic peaks at 409°C and 512°C during cooling cycle correspond to phase transition from β to α phase (β/α) and γ to β phase (γ/β), respectively. The transition temperatures are determined from the onset temperatures of endo-exothermic peaks. The transition temperatures have shifted to lower side during cooling cycle. The peak positions obtained from differential DTA are also in correlation with the peak positions obtained from DTA during heating and cooling cycles.

The weight change has been shown in the inset of Fig. 2(a) for sample x = 0.05. During heating, the first step occupies the region from room temperature till 340°C for which the weight loss occurred is attributed to the humidity. The second region from 340° to 800°C has shown abrupt increase in weight, which could be due to partial oxidation of different ions. During cooling, the temperature region 800°-480°C shows maximum weight loss, which could be due to partial reduction of ions. The temperature range 480°-1200°C is due to full reduction of ions as well as the final formation of solid-state oxide[26-28].

During heating the sample has been oxidized whereas during cooling the sample has been reduced. For x = 0.1, the transitions has been observed at 432°C (α/β) and 518°C (β/γ) during heating as is clear from Fig. 2(b). During cooling cycle, the transition

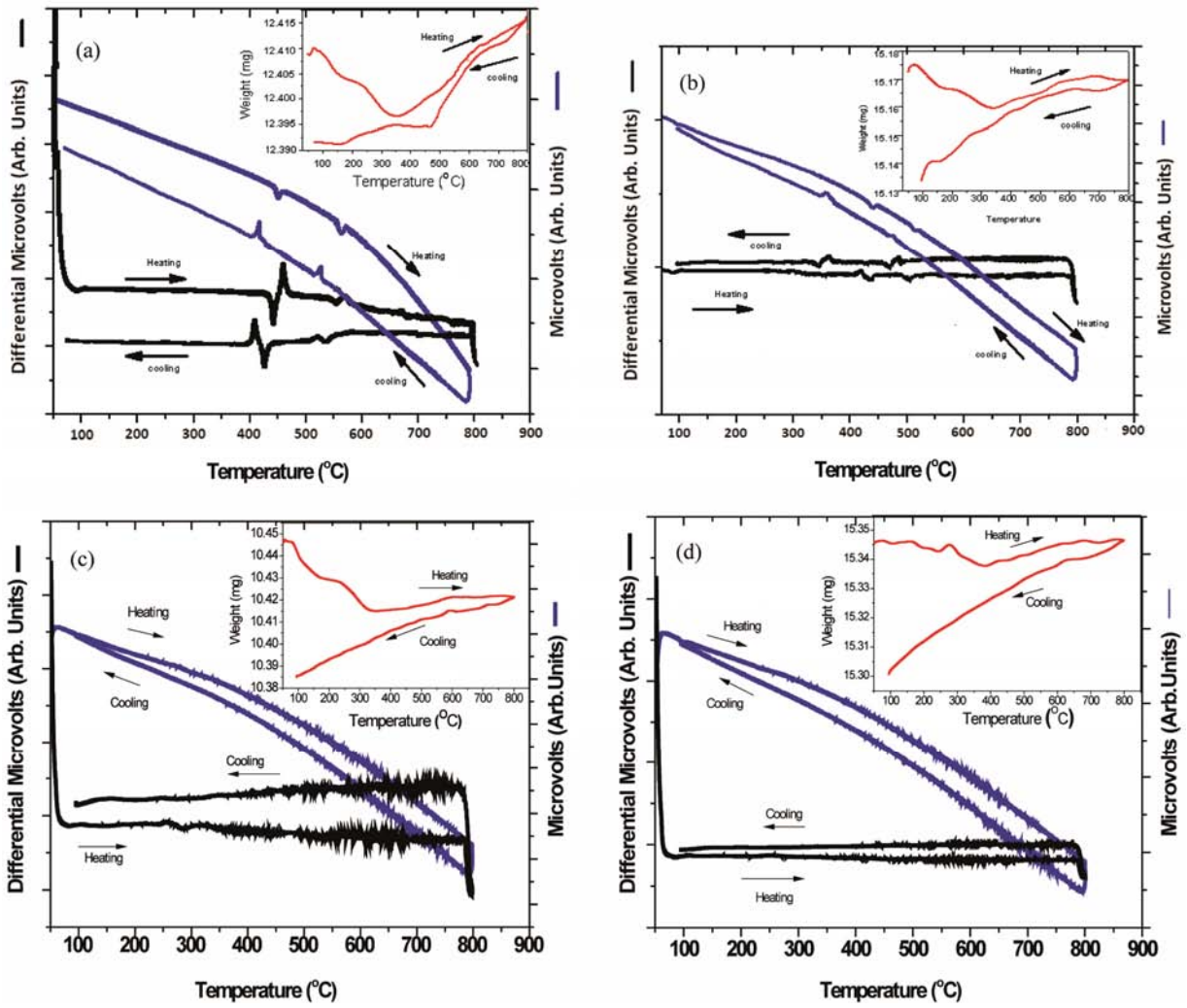

Fig. 2 — DTA, weight change and differential DTA for the sample (a) $x = 0.05$ ($Bi_2V_{0.95}Ti0_{.05}O_{5.5-\delta}$), (b) $x = 0.1$ ($Bi_2V_{0.90}Ti0_{.10}O_{5.5-\delta}$), (c) $x = 0.15$ ($Bi_2V_{0.85}Ti0_{.15}O_{5.5-\delta}$), (d) $x = 0.2$ ($Bi_2V_{0.80}Ti0_{.20}O_{5.5-\delta}$)

onset temperatures have shifted to 478°C (γ /β) and 367°C (β/α), respectively. In addition to this, the sharpness of peaks reduced in comparison to $x = 0.05$. Broad and small peaks represent continuous conductivity change (shown later). γ phase is stabilized against α and β with the widening of temperature region for γ as is indicated by the shift of phase transition points towards lower temperature during cooling cycle. For $x = 0.15$ and 0.2, γ is stabilized at room temperature as shown in Fig. 2(c-d). Both the samples show no evidence of (α/β) or (β/γ) transitions during heating or cooling cycle. Doping on V site increases the configurational entropy due to crystallographic distortion[1]. This has an advantage to thermodynamically stabilize γ phase against β or α phase in $Bi_2V\ O_{5.5-\delta}$. Hence, the presence of large amount of oxygen vacancies due to dopant in V-O layers retards the ordering from γ to β or α phase. For $x = 0.15$, a small inflection is observed at about 258°C during heating cycle which could be due to some structural relaxation induced by the rearrangement of oxygen vacancies[16,20]. The change in oxygen content from TGA has been calculated and listed in Table 1 for all the studied samples. Weight change is attributed basically to the change in oxygen content. For instance, the initial value of oxygen content of as-prepared sample $x = 0.15$ is regarded to be 10.447 and final value is 10.424 after reduction during heating cycle. Hence, the value for $\delta = 0.023$ for $x = 0.15$ during heating cycle.

From Table 1, it is very clear that the disorder in oxygen is increasing with dopant concentration during

heating and cooling cycle. Moreover, all the samples have shown reduction during the cooling cycle as is indicated by the weight change. Hence, Ti^{3+} must have not oxidized to Ti^{4+} as is indicated by the thermogravimetry.

3.3 Thermal expansion coefficient (TEC)

The dilatometry utilizes either transformation strains or thermal strains generating the basic data in the form of curves of dimension against time and temperature. The coefficient of linear expansion, also known as expansivity, is the ratio of the change in length per °C to the length at 0°C (dL/L_o). TEC is attributed to the asymmetric potential well in the systems[29]. Generally, deep potential wells are more symmetrical about the equilibrium position in comparison to shallow potential wells.

Thermal expansion for a given substance tends to be small for strongly bonded materials in comparison to weakly bonded materials. The plots between expansivity and differential of expansivity with respect to temperature are shown in Fig. 3(a-d). The technical thermal expansion coefficient has been calculated from the slope of expansivity versus temperature curve. The physical thermal expansion coefficient values have been calculated from the differential of expansivity curve. The physical TEC gives point value reaction i.e. the TEC can be evaluated at any temperature whereas technical TEC gives the TEC within a defined temperature range. The thermal expansion coefficient of the samples for different temperature regions is listed in Table 2.

The $Bi_2V_{.80}Ti_{.20}O_{5.5-\delta}$ oxide at 800°C exhibited higher TEC value than all other samples in present investigation indicating higher disorder/weak bonding in it. This means TEC value increased when the

Table 1 — Oxygen disorder in samples with heating or cooling

Sample Name	Heating	Cooling
$Bi_2V_{0.95}Ti_{0.05}O_{5.5-\delta}$	$Bi_2V_{.95}Ti_{.05}O_{5.509}$	$Bi_2V_{.95}Ti_{.05}O_{5.475}$
$Bi_2V_{0.90}Ti_{0.10}O_{5.5-\delta}$	$Bi_2V_{.90}Ti_{.10}O_{5.493}$	$Bi_2V_{.90}Ti_{.10}O_{5.469}$
$Bi_2V_{0.85}Ti_{0.15}O_{5.5-\delta}$	$Bi_2V_{.85}Ti_{.15}O_{5.477}$	$Bi_2V_{.85}Ti_{.15}O_{5.467}$
$Bi_2V_{0.80}Ti_{0.20}O_{5.5-\delta}$	$Bi_2V_{.80}Ti_{.20}O_{5.449}$	$Bi_2V_{.80}Ti_{.20}O_{5.456}$

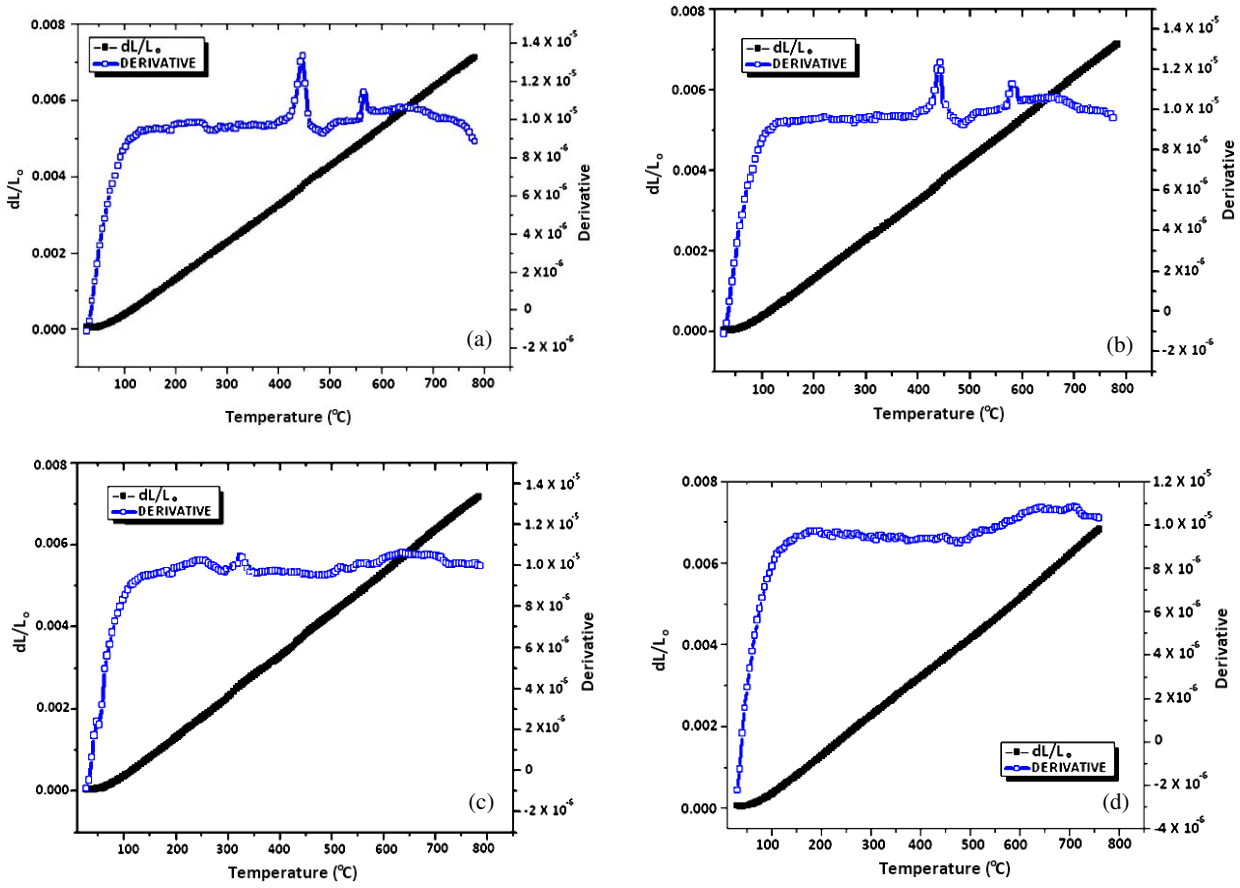

Fig. 3 — Expansivity and its derivative curves for the sample (a) $x = 0.05$ ($Bi_2V_{0.95}Ti0_{.05}O_{5.5-\delta}$), (b) $x = 0.1$ ($Bi_2V_{0.90}Ti0_{.10}O_{5.5-\delta}$), (c) $x = 0.15$ ($Bi_2V_{0.85}Ti0_{.15}O_{5.5-\delta}$) and (d) $x = 0.2$ ($Bi_2V_{0.80}Ti0_{.20}O_{5.5-\delta}$)

prepared oxide undergoes maximum structural rearrangement during maximum disorder. Yaremchenko *et al*[30]. reported the TEC for $Bi_{1.1}La_{0.1}V_{0.9}Cu_{0.1}O_{5.5-\delta}$ to be 15.5×10^{-6}/°C. For $Bi_{1.8}La_{0.2}V_{0.9}Cu_{0.1}O_{5.5-\delta}$, the TEC is obtained to be 14.3×10^{-6}/°C. The nickel doped samples exhibited lower TEC i.e. for $Bi_{1.8}La_{0.2}V_{0.8}Ni_{0.1}Cu_{0.1}O_{5.5-\delta}$ have TEC of 13.5×10^{-6}/°C. Usually, the SOFC materials should exhibit TEC between $(9\text{-}13)\times10^{-6}$/°C for chemical and interfacial compatibility among the components[31]. Hence, in the present investigation, all the doped samples have TEC in acceptable range though there is not much difference observed in the TEC of all the samples. In addition to this, the derivative curve of expansivity is of significance as the position of peaks represents the temperature of phase transitions.

From Fig. 3(a), it is clear that two peaks appear at 422°C and 552°C for $x = 0.05$, which corresponds to the phase transitions. Similarly, peaks at 416°C and 537°C have been obtained for $x = 0.10$ [Fig. 3(b)]. Only one peak appears at 304°C for $x = 0.15$ which could be due to some structural rearrangement. No peak appeared for $x = 0.20$ indicating the absence of any phase transition. The physical TEC corresponding to the phase transitions have been listed in Table 3.

α/β transition is having high TEC as compared to β/γ transition for both $x = 0.05$ and 0.10. The obtained results clearly indicated that the phase transition (α/β) region is more asymmetric and unstable than (β/γ) region. Whereas, no such transitions have been observed for $x = 0.15$ and 0.20. The results and various transitions obtained are in correlation with the thermal analysis results.

Table 2 — TEC of all the samples

Sample Name	Technical TEC from RT-800°C (/°C)	Technical TEC from 600°-800°C (/°C)	Physical value of TEC at 800°C (/°C)
$Bi_2V_{0.95}Ti_{0.05}O_{5.5-\delta}$	9.56×10^{-6}	9.73×10^{-6}	8.82×10^{-6}
$Bi_2V_{0.90}Ti_{0.10}O_{5.5-\delta}$	10.12×10^{-6}	9.82×10^{-6}	9.36×10^{-6}
$Bi_2V_{0.85}Ti_{0.15}O_{5.5-\delta}$	9.93×10^{-6}	9.89×10^{-6}	10.06×10^{-6}
$Bi_2V_{0.80}Ti_{0.20}O_{5.5-\delta}$	10.04×10^{-6}	9.91×10^{-6}	10.25×10^{-6}

Table 3 — TEC during phase transitions

Sample Name	α/β (/°C)	β/γ (/°C)
$Bi_2V_{0.95}Ti_{0.05}O_{5.5-\delta}$	13.8×10^{-6}	11.9×10^{-6}
$Bi_2V_{0.90}Ti_{0.10}O_{5.5-\delta}$	12.2×10^{-6}	11.2×10^{-6}
$Bi_2V_{0.85}Ti_{0.15}O_{5.5-\delta}$	10.4×10^{-6} at 302°C	
$Bi_2V_{0.80}Ti_{0.20}O_{5.5-\delta}$	No Transition	

3.4 Conductivity analysis

The electrical conductivity results in the form of Arrhenius plots are shown in Fig. 4(a) for the synthesized phases which clearly manifests the transition temperatures for all dopings i.e. $0.05 \le x \le 0.20$. For $x = 0.05$ and 0.10, the Arrhenius plots of conductivity clearly shows three transition regions attributed to three principle polymorphs of $Bi_2VO_{5.5-\delta}$. For $x = 0.05$, the sample exhibits pronounced conductivity jump near 442°C and 541°C which are related to (β/α) and (γ /β) transitions as also observed in TEC and DTA measurements. Similar transitions have been observed for $x = 0.10$ at 386° and 488°C, respectively. For $x = 0.15$, the conductivity jump for (β/α) have almost disappeared along with a small change in slope.

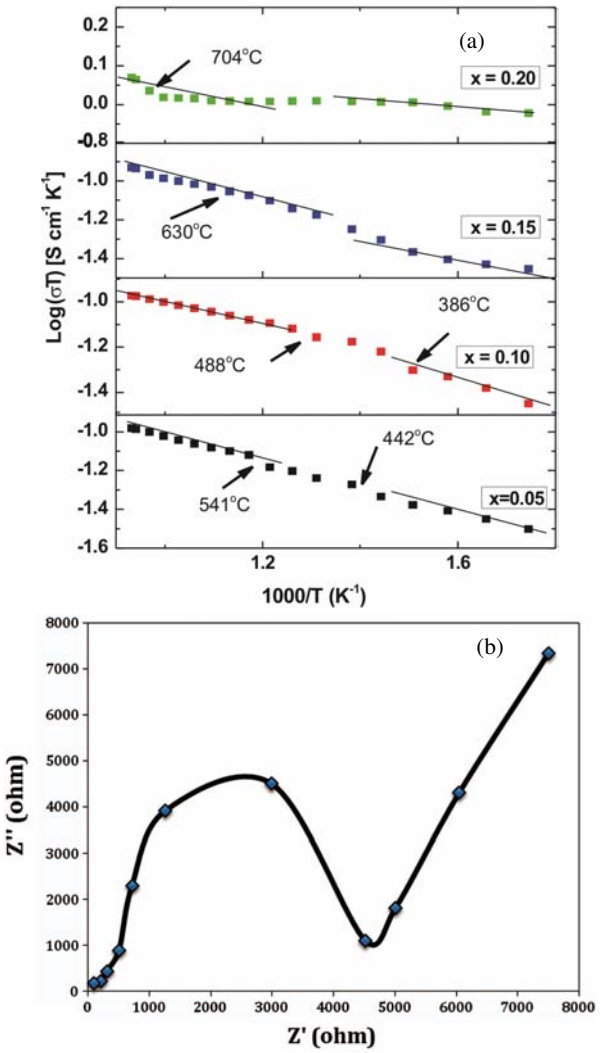

Fig. 4 — (a) Arrehnius plots for all the samples indicating phase transitions during cooling cycles and (b) Cole-Cole plot for sample $x = 0.1$ at temperature 500°C

However, continuous jump from low conducting to high conducting state is observed at 630°C, which could be due to some structural relaxation. Doping with x = 0.20 leads to disappearance of (β/α) and (γ/β). Only a small inflection at 704°C is observed which again could be related to oxygen relaxation during phase change[32,33] from γ′ to γ. Hence, small difference in atomic arrangement can notably change the transition behaviour. The results obtained from DTA and dilatometry is found to be in well agreement with conductivity results. The conductivity was calculated using the formula:

$$\sigma = l/RA \quad \ldots (3)$$

where l is the thickness of the pellet, A is the area of cross-section of gold sputtered pellet and R is the total resistance of sample calculated from the point of intersection of Cole-Cole semicircle plot on the real axis. The representative plot for Cole-Cole plot for sample x= 0.1 at temperature 500°C is shown in Fig. 4(b). The electrical conductivities at different temperatures as well as activation energies are listed in Table 4.

Activation energy can be obtained from the slope of the Arrhenius line. Break in Arrhenius plots also signify the corresponding change in activation energy for conduction. From Table 4, it is clear that activation energy of conduction is higher for low temperatures. The change in activation energy is also associated with association-dissociation of defect clusters[34,35]. The sample x = 0.20 exhibits highest conductivity of 1.17×10^{-3} S/cm at 800°C. This could be due to polaron hopping, vacancy concentration as well as optimization of pathways for O^{2-}ion motion. The conductivity of x = 0.20 at 800°C exceeds that of x = 0.05 by two orders of magnitude. Similar trend of conductivity has been observed at 600°C. In addition to this, the conductivity of x = 0.20 changes only by an order of magnitude from x = 0.05 at 400°C. This can be due to small thermal energy at low temperatures to promote the migration of oxygen. Above 400°C, the conductivity rises due to thermal activation. The sample x = 0.20 shows two order higher conductivity[18]. It may be ascribed to good theoretical density than earlier reported density. In summary, it indicates that the processing conditions play very important role to decide the transport properties.

For solid electrolytes, the electrical conductivity shows dependence on frequency as shown in Fig. 5. This is known as Jonscher's power law according to which there are three regions i.e low frequency region, an intermediate frequency and high frequency region[36,37]. In the low frequency region, the conductivity is mainly due to the polarization effect between the electrode and electrode surface. When the frequency drops, the charge accumulation at electrode/electrolyte surface increases which decreases the conductivity. In the intermediate

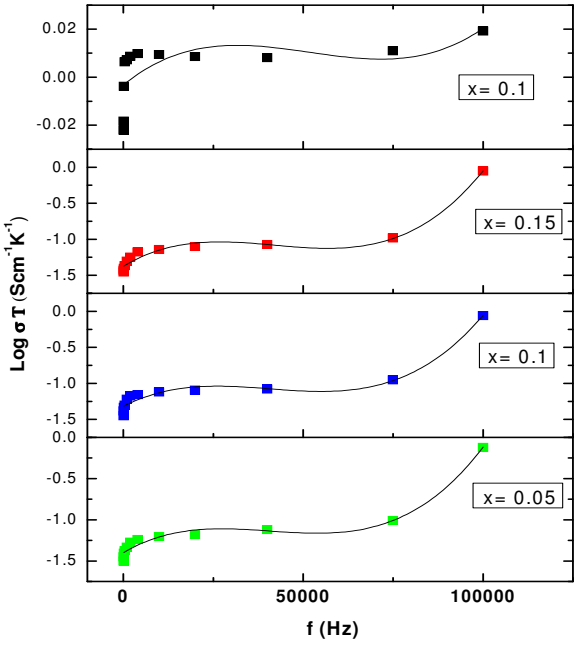

Fig. 5 — Plot of frequency with conductivity demonstrating Jonscher's power law

Table 4 — Conductivity and activation energy for samples

Sample Name	σ (S/cm) at 400°C	σ(S/cm) at 600°C	σ_{800} (S/cm) at 800°C	E_a <400°C (in eV)	E_a > 500°C (in eV)	Density (g/cc)
$Bi_2V_{0.95}Ti_{0.05}O_{5.5-\delta}$	6.71×10^{-5}	9.01×10^{-5}	9.74×10^{-5}	0.29	0.22	7.42
$Bi_2V_{0.90}Ti_{0.10}O_{5.5-\delta}$	7.71×10^{-5}	9.11×10^{-5}	9.67×10^{-5}	0.27	0.20	7.38
$Bi_2V_{0.85}Ti_{0.15}O_{5.5-\delta}$	8.71×10^{-5}	1.11×10^{-4}	1.78×10^{-4}	0.31	0.24	7.29
$Bi_2V_{0.80}Ti_{0.20}O_{5.5-\delta}$	1.71×10^{-4}	1.08×10^{-3}	1.17×10^{-3}	0.25	0.19	7.31

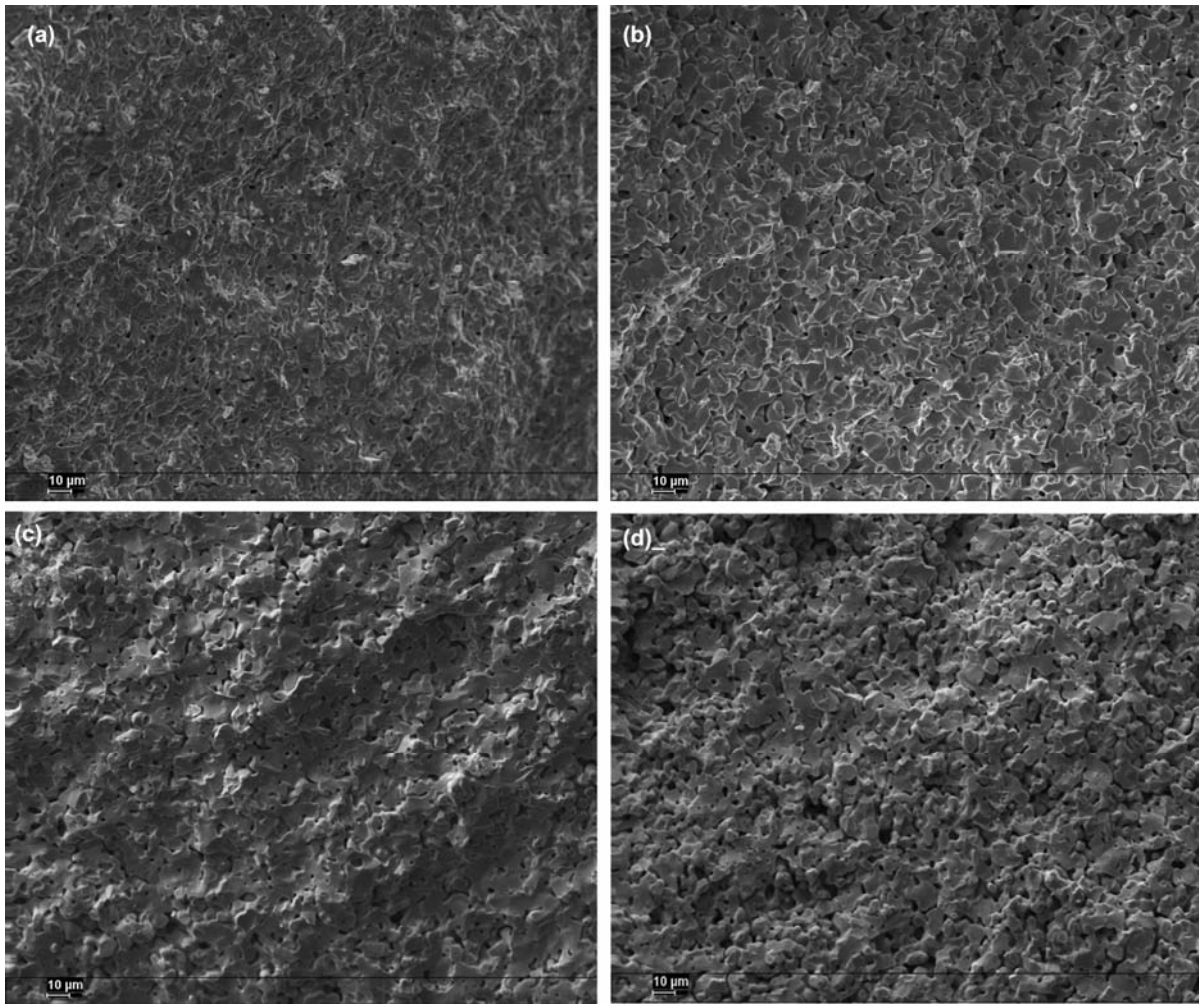

Fig. 6 — Microstructure of the sample (a) $x = 0.05$ ($Bi_2V_{0.95}Ti0_{.05}O_{5.5-\delta}$), (b) $x = 0.1$ ($Bi_2V_{0.90}Ti0_{.10}O_{5.5-\delta}$), (c) $x = 0.15$ ($Bi_2V_{0.85}Ti0_{.15}O_{5.5-\delta}$) and (d) $x = 0.2$ ($Bi_2V_{0.80}Ti0_{.20}O_{5.5-\delta}$)

frequency region, the conductivity is almost independent of frequency whereas the conductivity increases in the high frequency region.

3.5 Microstructure and grain size

The fractured surface of $Bi_2V_{1-x}Ti_xO_{5.5-\delta}$ ($0.05 \leq x \leq 0.20$) has been analyzed by SEM and shown in Figs. 6(a-d), respectively. The porosity as well as grain size increased with dopant concentration. The microstructures for $x \leq 0.1$ [Fig. 6(a-b)] exhibited cluster like non-uniform pattern with subsequently decreased porosity, which are found to be in well agreement with the results obtained for density. However, the particles are well connected to each other having well bone porous network. From Fig. 6(d), it is clearly depicted that the most homogenous pattern is observed for $Bi_2V_{0.80}Ti0_{.20}O_{5.5-\delta}$. The grains are found to be more uniform with observable porosity for this sample. No segregation of elements in the bulk materials is observed except for $x = 0.25$. As the dopant concentration increased from $x = 0.05$ to $x = 0.20$, the grain size subsequently increased for all the samples. The grain size, standard deviation and variance up to ± 0.001 are listed in Table 5. Standard deviation gives variation or dispersion from the average value. The

Table 5 — Grain size, standard deviation (σ) and variance (σ^2)

Sample Name	Average Grain Size (µm)	Standard deviation (σ)	Variance (σ^2)
$Bi_2V_{0.95}Ti_{0.05}O_{5.5-\delta}$	3.31	1.56	2.44
$Bi_2V_{0.90}Ti_{0.10}O_{5.5-\delta}$	3.90	1.78	3.17
$Bi_2V_{0.85}Ti_{0.15}O_{5.5-\delta}$	5.23	1.44	2.07
$Bi_2V_{0.80}Ti_{0.20}O_{5.5-\delta}$	7.74	1.51	2.28

sampling of 50 grains is done to obtain the average grain size and subsequently standard deviation. Low standard deviation for $Bi_2V_{0.85}Ti_{0.15}O_{5.5-\delta}$ indicates that the data points tend to be very close to the mean and clustered around it. High standard deviation for $Bi_2V_{0.90}Ti_{0.10}O_{11-\delta}$ indicates that the data are spread out over a large range of values.

Grain size is found to be highest for $Bi_2V_{0.80}TI_{0.20}O_{5.5-\delta}$ and lowest for $Bi_2V_{0.95}Ti_{0.05}O_{5.5-\delta}$. The structural stability and homogeneity of these samples are likely to have dominating impact on their conductive as well as thermal properties.

4 Conclusions

High conducting γ phase is stabilized for $x = 0.15$ and $x = 0.20$ at room temperatures which is evident from XRD as well as thermal analysis results. Sample $x = 0.20$ has shown maximum conductivity i.e. 1.17×10^{-3} S/cm and minimum activation energy of 0.19 eV at 800°C. In addition to this, the grain size has increased with dopant concentration. The $Bi_2V_{0.80}Ti_{0.20}O_{5.5-\delta}$ oxide at 800°C exhibited higher TEC value than all other samples in present investigation indicating higher asymmetric potential well. All the samples have shown reduction during the cooling cycle indicating that Ti^{3+} must have not oxidized to Ti^{4+}. The porosity as well as grain size increased with dopant concentration and the high density of samples is obtained. The microstructures for $x \leq 0.1$ exhibited cluster like non-uniform pattern with subsequently decreased porosity.

Acknowledgement

The authors are thankful to DST (SR/WOS-A/PS-23/2009), New Delhi for financial assistance. One of the authors GK is thankful to Dr Vishal Kumar, SGGSWU, Fatehgarh Sahib for his consistent guidance.

References

1 Taninouchi Y K, Uda T & Ichitsubo T, *Solid State Ionics*, 181 (2010) 719.
2 Abraham F, Boivinb J C & Mairesse G, Nowogrocki G, *Solid State Ionics*, 934 (1990) 40.
3 Boivin J C & Mairesse G, *Chem Mater*, 10 (1998) 2870.
4 Yan J & Greenblatt M, *Solid State Ionics*, 81 (1995) 225.
5 Dygas J R, Krok F, Bogusz W, Kurek P, Reiselhuber K & Breiter M W, *Solid State Ionics*, 239 (1994) 70.
6 Greenblatt M, *Ionic Conductors*, 33 (1999) 1584.
7 Lee C K, Sinclair D C & West A R, *Solid State Ionics*, 62 (1993) 193.
8 Cho H S, Sakai G, Shimanoe K & Yamazoe N, *Sens Actuators B*, 109 (2005) 307.
9 Culea E, *J Non-Cryst Solids*, 223 (1998) 147.
10 Zhen Q, Kale G M, Shi G, Li R, He W & Liu J, *Solid State Ionics*, 176 (2005) 2727.
11 Lofberg A, Bodet H, Pirovano C, Steil M C, Vannier R N & Bordes-Richard E, *Catal Today*, 118 (2006) 223.
12 Zyryanov V V, *J Struct Chem*, 45 (2004) 133.
13 Pasciak G, Chmielowiec J & Bujło P, *Mater Sci Poland*, 23 (2005) 209.
14 Kant R, Pandey O P & Singh K, *Int J Hydro Energy*, 33 (2008) 455.
15 Kaur G, Pandey O P & Singh K, *Phys Status Sol A*, 209 (2012) 1231.
16 Kant R, Pandey O P & Singh K, *Ionics*, 10 (2010) 277.
17 Shannon R D, *Acta Crystall Sect A*, 32 (1976) 751.
18 Kant R, Pandey O P & Singh K, *Mater Sci Engg B*, 158 (2009) 63.
19 Paulin P I, Morelli M R & Maestrelli S C, *Mat Res Innovat*, 3 (2000) 292.
20 Vinke I C, Diepgrond J, Boukamp B A, de Vries K J & Burggraaf A J, *Solid State Ionics*, 57 (1992) 83.
21 Vannier R N, Mairesse G, Abraham F, Nowogrocki G, Pernot E, Anne M, Bacmann M & Strobel P, J Fouletier, *Solid State Ionics*, 78 (1995) 183.
22 Vannier R N, Mairesse G, Abraham F & Nowogrocki G, *Solid State Ionics*, 80 (1995) 11.
23 Vannier R N, Mairesse G, Abraham F & Nowogrocki G, *Solid State Chem*, 103 (1993) 441.
24 Lazure S, Vernochet Ch, Vannier R N, Nowogrocki G & Mairesse G, *Solid State Ionics*, 90 (1996) 117.
25 Abrahams I, Krok F, Malys M & Wrobel W, *Solid State Ionics*, 176 (2005) 2053.
26 Sekkina M A & Elsabawy K M, *Phys C*, 377 (2002) 254.
27 Rao Y Srinivasa & Sunandana C S, *J Mater Sci*, 11 (1992) 595.
28 Tahar R H, Tahar N H & Salah A B, *J Crystal Growth*, 307 (2007) 40.
29 Raghvan V, Materials Science & Engineering, 5th Edition, (2008) 74.
30 Yaremchenko A A, Kharton V V, Naumovich E N & Samokhval V V, *Solid State Ionics*, 111 (1998) 227
31 Tietz F, *Ionics*, 5 (1995), 129.
32 Pernot E, Anne M, Bacmann M, Strobel P, Fouletier J, Vannier R N, Mairesse G, Abraham F & Nowogrocki G, *Solid State Ionics*, 259 (1994) 70.
33 Watanabe A & Das K, *J Solid State Chem*, 163 (2002) 224.
34 Tuller H, Schoonman J & Riess I (Eds), Kluwer (NATO ASI), Dordrecht, (2000) 245.
35 Chmielowiec J, Pasciak G & Bujlo P, *Mater Sci-Poland*, 27 (2009) 1251.
36 Joncher A K, *Phys Thin Films*, 11 (1980) 231.
37 lngram M D, *Phys Chem Glasses*, 28 (1987) 215.